Lithosphere

Research Article

Cross-Scale Study of the High-Steep Reservoir Banks under Different Mechanical States

Yulin Zou [1,2] **Wengang Zhang** [1,3] **Luqi Wang** [1,3] **Xuecheng Gao** [1,3,4] **and Wang Lu** [1,3]

[1]*School of Civil Engineering, Chongqing University, Chongqing 400045, China*
[2]*Sichuan Yanjiang Panning Expressway Co., Ltd., Panzhihua, 617000 Sichuan, China*
[3]*National Joint Engineering Research Center of Geohazards Prevention in the Reservoir Areas, Chongqing 400045, China*
[4]*Industrial Technology Research Institute, Chongqing University, Chongqing 400045, China*

Correspondence should be addressed to Luqi Wang; wlq93@cqu.edu.cn

The deformation of high-steep rocky banks is caused by the self-weight of overlying rock mass and the fluctuation of reservoir water. In this paper, the newly developed testing equipment and the particle flow code (PFC) were used to complete the cross-scale study of the high-steep rocky banks under different mechanical states. The test conditions involved the dry state, saturated state, and hydraulic coupling states under different confining pressures. Combined with the micrographs of the fractured surface under different mechanical states, it can be found that the participation of the water could reduce the bond contact and accelerate the deformation of the particles, ultimately leading to an increase in the plastic deformation and a decrease in the peak strength of the rock mass. Compared to the saturated state, the water in the hydraulic coupling state was not transferred though the storage space was compressed; thus, the water pressure would further promote the extension of the microcracks. When considering the fluctuations of the reservoir water, the changes in the mechanical state may accelerate the degradation rate of the rock mass. The related methods can provide data support and a theoretical basis to the evolution trend of high-steep rocky reservoir banks.

1. Introduction

Since the implementation of experimental water storage in the Three Gorges Reservoir area in 2008, the highest controlled water level was 175 m, and the lowest controlled water level was 145 m. With the increase of numbers of reservoir water level fluctuations, a degradation zone up to 30 m height is developed on both reservoir banks [1, 2]. The rocks in the degradation zone have been in a complex dynamic mechanical environment, leading to degradations at a visible rate [3, 4]. And this deterioration trend becomes a key factor inducing the instability of the high-steep reservoir banks in the current stage [5–7]. Specifically, the foot of the high-steep reservoir bank is located in the degradation zone. During the fluctuations of the reservoir water, the base rock mass circulates between two ultimate states, namely, the dry state and the hydraulic coupling state [8, 9].

In the current test method, to establish a hydraulic coupling environment, the rock is generally wrapped in a rubber membrane, and seepage pressure is applied to one side of the rock to form a pressure difference [10–13]. However, there is a large gap between this test method and the hydraulic coupling environment of the base rock mass on the reservoir bank, and it has become an obstacle to further exploring the mechanical properties of rocks in a complex mechanical environment. It should be noted that the hydraulic coupling state of high-steep rocky banks under actual working conditions is a special mechanical environment without lateral restraint [14]. Due to the fluctuations of the reservoir water, the water pressure is also continuously changing.

In this study, newly developed testing equipment was used to perform hydraulic coupling tests without lateral restraint. Based on the results of the experiments and particle flow code (PFC), cross-scale analysis of the high-steep
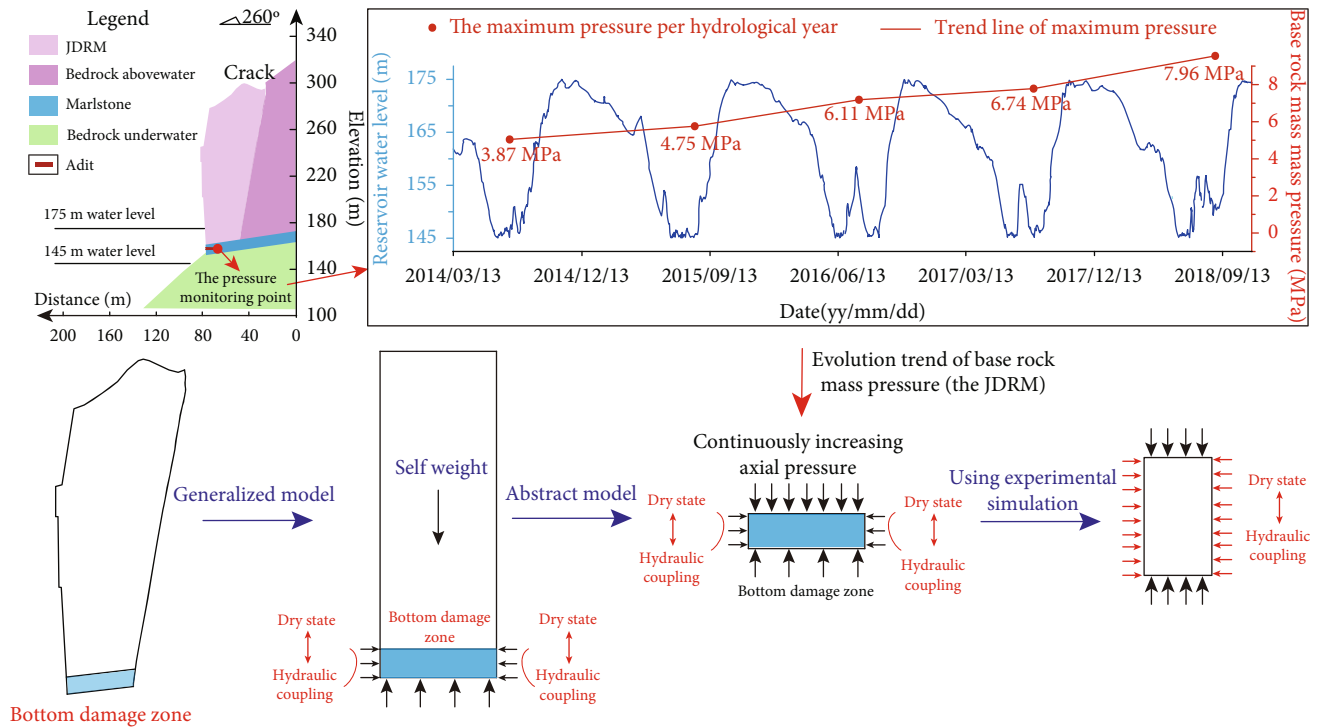
FIGURE 1: The mechanical model of the high-steep rocky reservoir bank.

rocky bank under different mechanical states was conducted, including the dry state, saturated state, and hydraulic coupling state under different confining pressures. These working conditions basically cover the key mechanical states under the fluctuation of reservoir water, providing data support and a theoretical basis for determining the evolution trend of high-steep rocky reservoir banks.

2. Generalization of the Mechanical Model and the Experimental Method

Taking the Jianchuandong dangerous rock mass (JDRM) in the Three Gorges Reservoir area as an example, the mechanical model of the rocky reservoir bank in the high-steep canyon area could be obtained (Figure 1). Specifically, the middle-upper part was robust with fewer cracks than the foot of the rocky bank. Mechanical analysis showed that the self-weight of the middle-upper part could be simplified to the axial compressive pressure. Moreover, the basal area could be generalized using a damage model that incorporates long-term axial stress and the fluctuations of the reservoir water [15]. The monitoring data indicated that the base rock mass pressure continued to increase with the fluctuation of reservoir water. Therefore, a uniaxial compression test was applied to simulate the dry state, and hydraulic coupling tests with different water pressures were used to simulate the rise and fall of the reservoir water level. This type of test could reflect the continuously increasing axial pressure and the progressive deformation of high-steep rocky bank. Notably, the focus of this study was the mechanical properties of the rocky reservoir bank under different mechanical

states, so the continuity of the transition between mechanical states was not considered.

A multiscale mechanical experimental system (HMC-1000-60) was used to study the effect of the hydromechanical coupling (Figure 2). For the subject studied in this paper, the most significant advantage of this equipment lies in the application of hydraulic coupling. The water is directly used to apply the confining pressure to the rock mass, which can accurately represent the water-stress environment of the rocky reservoir bank. A detailed description of this apparatus can be found in Liu et al. [16] and Zhou et al. [17].

2.1. Analysis of the Macrostrength. Based on the mechanical model of the high-steep rocky bank, the rock samples under five mechanical states were tested. These five mechanical environments included uniaxial compression in the dry state, uniaxial compression in the saturated state, and hydraulic coupling under confining pressures of 0.3 MPa, 1 MPa, and 3 MPa. The maximum water level difference in the Three Gorges Reservoir area is 30 m, which corresponds to a water pressure of 0.3 MPa. Therefore, we focused on a water pressure of 0.3 MPa [9]. Then, confining pressure was increased by three times [12, 18], and the hydraulic coupling states under 1 MPa and 3 MPa were further analyzed. The saturated state was mostly used in the conventional dry-wet cycle test [8, 19], and it was used as a control group to reveal the mechanical properties of the rocky reservoir bank. Specifically, the samples were naturally soaked in water for 48 h to achieve the saturated state [15, 20, 21]. A comparison of different testing conditions is shown in Figure 3.
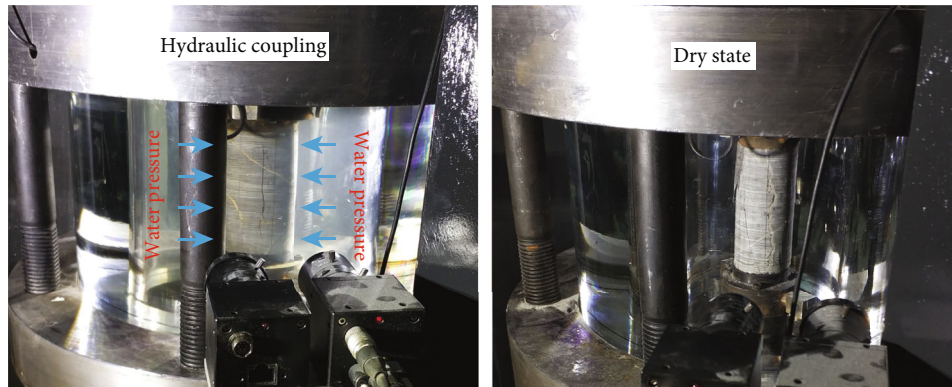
FIGURE 2: The experimental system for the mechanical model.

Uniaxial compression
(dry state)

Uniaxial compression
(saturated state)

Hydraulic coupling
(0.3 MPa)

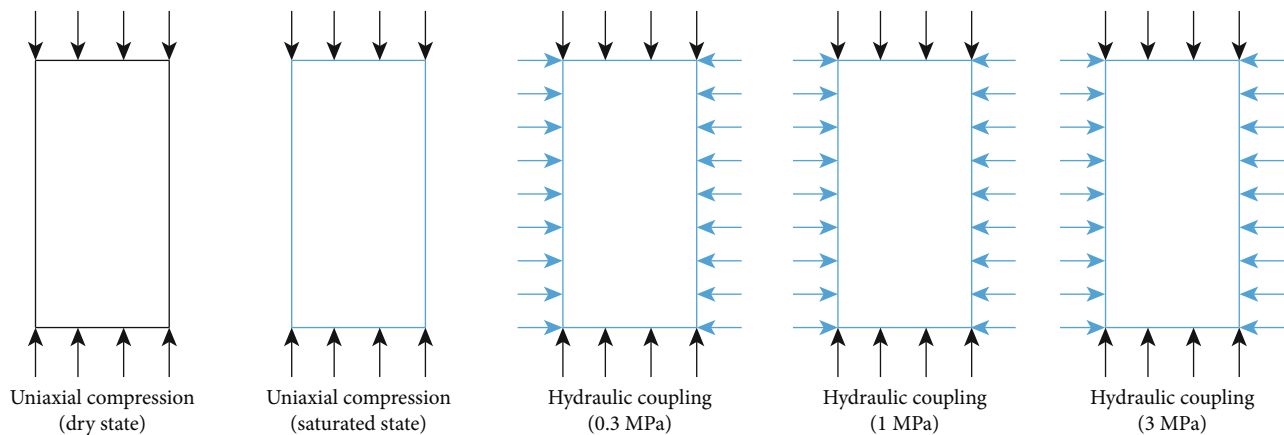Hydraulic coupling
(1 MPa)

Hydraulic coupling
(3 MPa)

FIGURE 3: Comparison of the testing conditions.

The samples were limestone collected from the degradation zone in the Three Gorges Reservoir area. Three samples were tested in each mechanical state, and the typical test curves under different testing conditions were compared during the analysis (Figure 4).

For the dense limestone used in the tests, the uniaxial compressive strength was 5.10% lower in the saturated state than in the dry state, but this decrease could be neglected. This indicated that the saturated state had less effect on the strength of the dense limestone. However, the strain corresponding to the saturated state's peak strength was higher than that of the dry state, indicating that the plasticity of the limestone increased in the saturated state. This difference in plasticity may be amplified when the rock mass was converted between the dry and saturated states.

Under the hydraulic coupling mechanical conditions of a low confining pressure (0.3 MPa), the strength of the limestone would be further reduced compared to that of the saturated state. Specifically, the strength of the limestone in the 0.3 MPa hydraulic coupling state was 3.64% lower than that in the saturated state, and it was 8.56% lower than that in the dry state. This phenomenon revealed that the participation of the water increased under hydraulic coupling. And the mechanical state of hydraulic coupling could soften the rock's particles and accelerate the failure process through the existing microdamage.

As the confining pressure continued to increase, the peak strength of the limestone gradually increased. In terms of the actual working conditions, the peak strength of the rock mass in the deep-water area was higher than that in the shallow-water area. Although the peak strength of the rock mass increased, the amount of plastic deformation continued to increase. The relevant analysis will be further analyzed after obtaining the microscopic parameters via numerical simulation.

2.2. Quantitative Study of the Microparameters. At present, with the development of computer technology, many numerical calculation methods have been introduced to analyze the evolution process [22, 23] and regional distribution of natural hazards [24, 25]. Compared to the continuum mechanics methods [26, 27], PFC can be used to study the mechanical properties and behavior of the elements from the perspective of microstructure [28, 29]. To be specific, the PFC can simulate the movement of and interactions between finite-sized particles. These particles are defined as rigid elements with finite masses that move independently of one another and can both translate and rotate. The particles interact at pair-wise contacts through the internal forces and moments. The contact mechanics are embodied in the particle-interaction laws that update the internal forces and moments. The time evolution of this system is computed
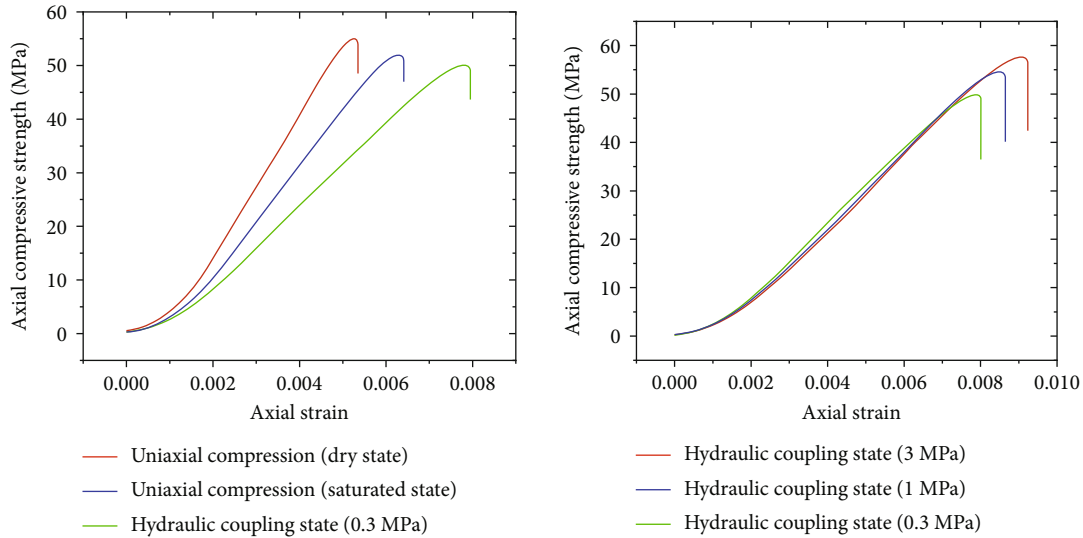
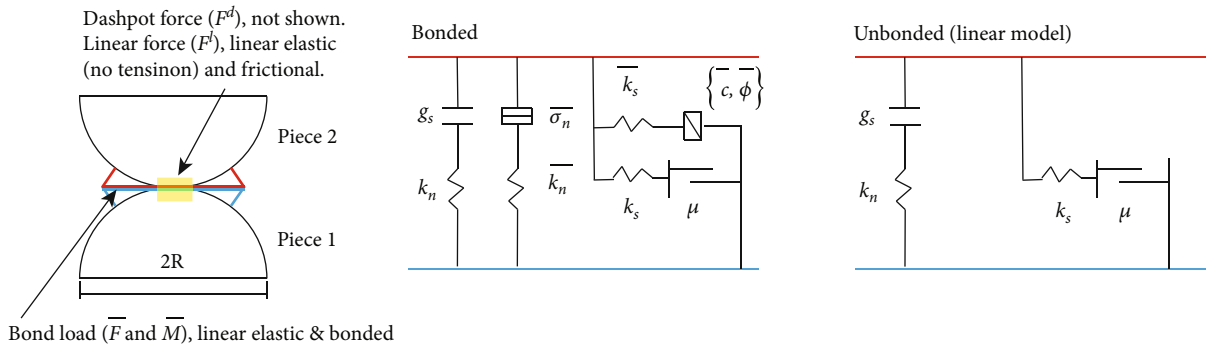FIGURE 4: The stress-strain curves under different mechanical states.

FIGURE 5: The constitutive model of the LPBM. g_s is the surface gap, k_n is the normal stiffness of the linear bond, k_s is the shear stiffness of the linear bond, μ is the friction coefficient of the linear bond, $\bar{k}_n$ is the normal stiffness of the parallel bond, $\bar{k}_s$ is the shear stiffness of the parallel bond, $\bar{\sigma}_c$ is the tensile strength of the parallel bond, $\bar{c}$ is the cohesion of the parallel bond, and $\bar{\phi}$ is the friction angle of the parallel bond.

via the distinct-element method, which provides an explicit dynamic solution to Newton's laws of motion. The PFC model provides a synthetic material consisting of an ensemble of rigid grains that interact at contacts and include granular and bonded materials [30–32].

The linear parallel bond model (LPBM) was used to define the contact relationships between the particles in the numerical calculations. This bond model is primarily employed to simulate materials such as rock and concrete. And it has the characteristics of a high bond strength and can withstand bending moments and other loads.

There are two interfaces of LPBM: an infinitesimal, linear elastic (no-tension), frictional interface that carries a force and a finite-size, linear elastic, bonded interface that carries a force and moment (Figure 5). Generally, the first interface is equivalent to the linear model. When the second interface is bonded, it resists the relative rotation, and its behavior is linear and elastic until the strength limit is exceeded and the bond breaks, making it unbonded. If the second interface is unbonded, it carries no load.

According to the macrotest data, the numerical simulation parameters were calibrated through multiple corrections. Thus, the numerical model can realistically reflect the loading process of the sample and link the macromechanical parameters to the microparameters. Based on the constitutive relationship of the LPBM, the calibration of the microparameters followed these principles:

(i) The parallel bond model degenerated into a linear contact model after the bond was broken. Therefore, when the sample was under tension or compression, the parallel bond part worked, but its deformation modulus was different. The linear contact part only worked when the sample was pressed

(ii) Poisson's ratio of the elastic deformation was affected by the normal-to-shear stiffness ratio, and these two parameters were linearly related

(iii) The value of the effective bond modulus was determined by the elastic modulus, and these two parameters were linearly related
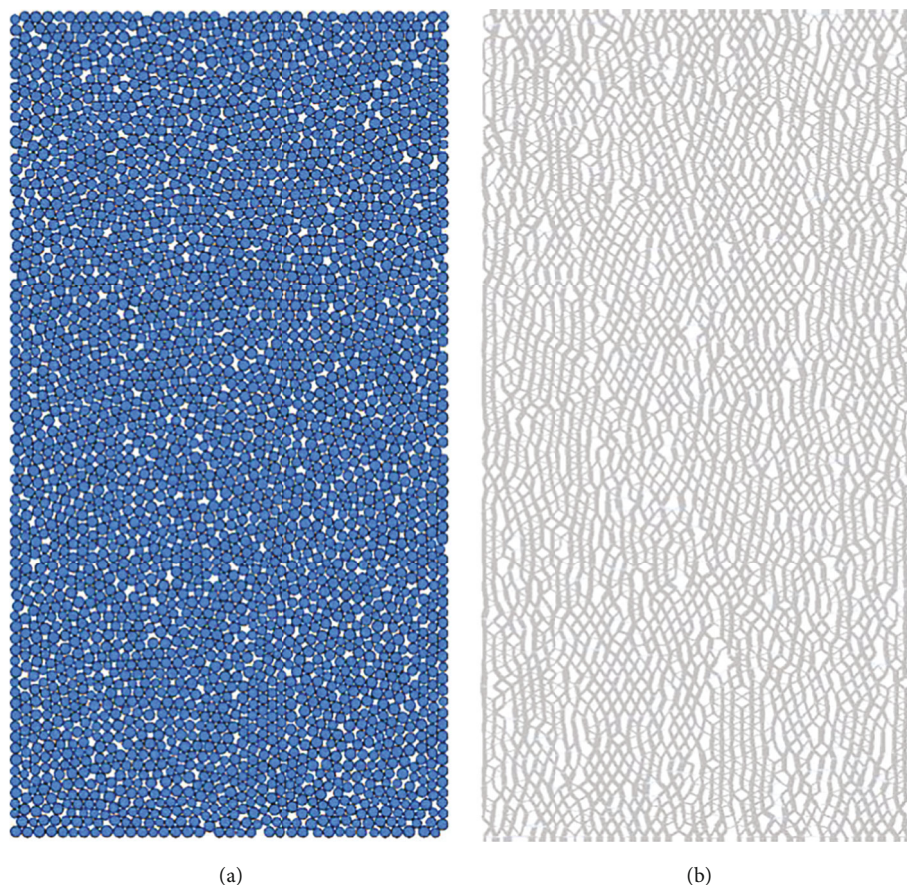
Figure 6: The numerical model of the particle flow. (a) The particle diagram of numerical model. (b) The force bond diagram of numerical model.

(iv) The failure mode of the sample was determined by the normal-to-shear stiffness ratio

(v) After the normal-to-shear stiffness ratio of the bond was determined, the amplification factor of the microscopic bonding parameter was linearly related to the axial compressive strength

In the process of constructing the numerical model, the porosity was set to 0.01; the diameter of the particle unit was set as 0.6–0.8 mm; and then, a 2D model with a diameter of 50 mm and a height of 100 mm was established. There were 3186 particles and 8078 initial contacts in this numerical model. The same physical model was used to quantitatively analyze the microparameters in the different mechanical states. The calculation model constructed using the PFC is shown in Figure 6.

Compression tests and tensile tests were conducted to analyze the mechanism of the macrosettings under corresponding microparameters. Due to the mutual influence of each parameter, it was necessary to further modify the contact model's microparameters. In the initial compaction stage (strain of less than 0.002), the related elastic modulus was about 10% of the linear stage's elastic modulus. This feature was simulated through the PFC programming. The numerical simulation experiments of the remaining four mechanical states were also

carried out using the same method. The relevant numerical results are shown in Figure 7.

As can be seen from the comparison, the results of the numerical simulation are in good agreement with the experimental data, and the corresponding law of the mechanical properties of the sample can be realized from a microscopic perspective. This method provides data support to the quantitative analysis of the characteristics under different mechanical states.

2.3. Cross-Scale Analysis of the Mechanical Properties. During the numerical experiments, the compressive strength, tensile strength, and cohesion strength were extracted to reflect the macromechanical properties of the rock mass. And the effective modulus, the bond effective modulus, the normal-to-shear stiffness ratio, and the bond normal-to-shear stiffness ratio were used to define the microcharacteristics of the particles. The relevant mechanical parameters involved in the numerical simulation are shown in Table 1. The trends of the parameters related to strength and deformation are shown in Figure 8.

By combining the constitutive relationship of the LPBM and the sensitivity analysis of the critical micro-parameters, the mechanical properties under the different states can be summarized as follows.
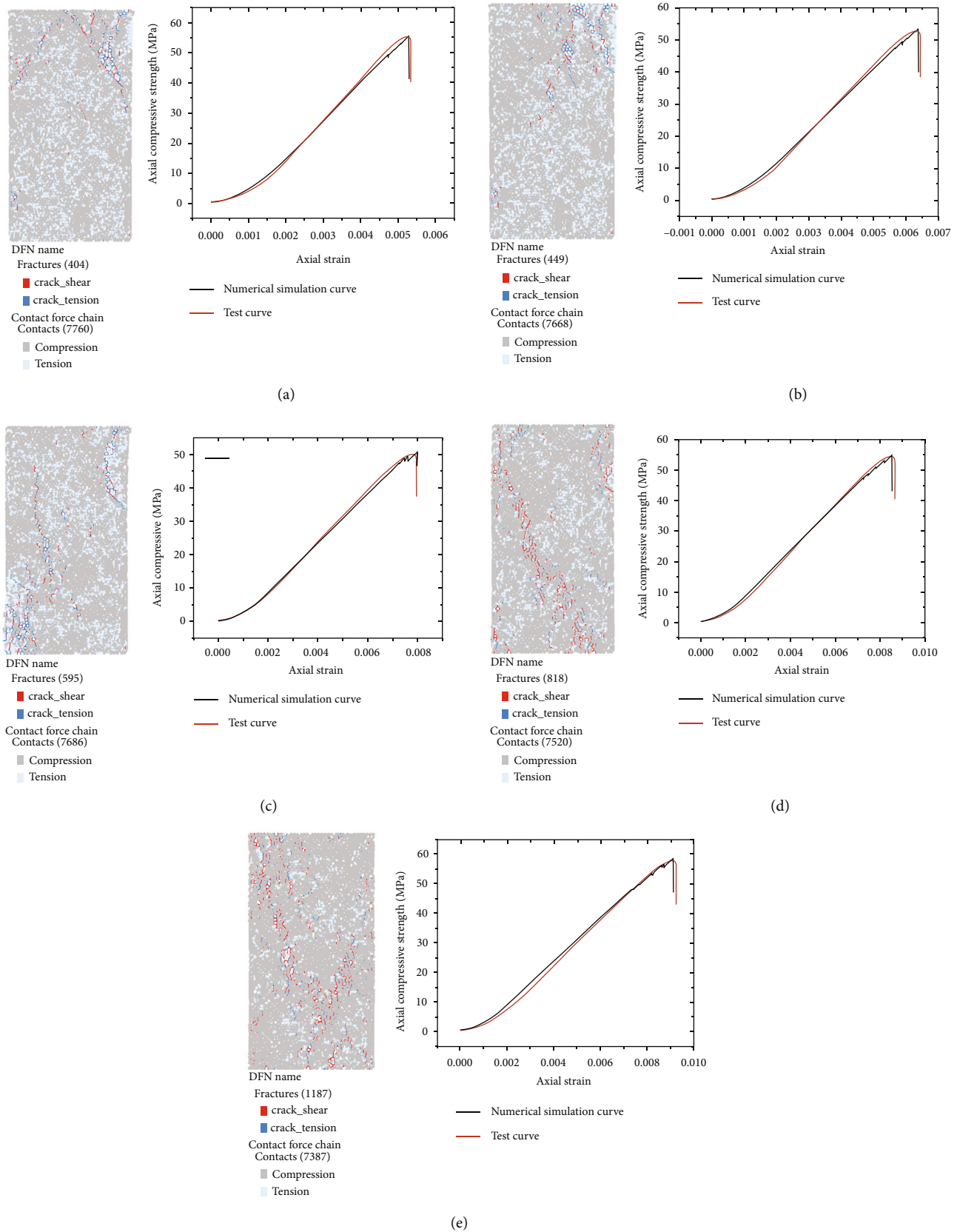
(a)

(b)

(c)

(d)

(e)

Figure 7: Comparison of the numerical simulation results. (a) Uniaxial compression in the dry state. (b) Uniaxial compression in the saturated state. (c) Hydraulic coupling under a confining pressure of 0.3 MPa. (d) Hydraulic coupling under a confining pressure of 1 MPa. (e) Hydraulic coupling under a confining pressure of 3 MPa.

Table 1: Parameters under different mechanical states (obtained from the numerical simulation).

(a)

The macroparameters	Uniaxial compression in dry state	Uniaxial compression in saturated state	Hydraulic coupling (0.3 MPa)	Hydraulic coupling (1 MPa)	Hydraulic coupling (3 MPa)
Peak intensity (MPa)/test data	54.9	52.1	50.2	54.5	58.6
Poisson's ratio/test data	0.25	0.25	0.26	0.26	0.26
Elastic modulus (GPa)/test data	12.5	9.82	7.5	7.42	7.21
Tensile modulus (GPa)/theoretical data	9.615	7.262	5.762	5.707	5.54

(b)

| The microparameters	Uniaxial compression in dry state	Uniaxial compression in saturated state	Hydraulic coupling (0.3 MPa)	Hydraulic coupling (1 MPa)	Hydraulic coupling (3 MPa)
Effective modulus (GPa)	6.518	5.112	2.845	2.78	1.532
Bond effective modulus (GPa)	6.615	4.852	4.373	4.351	4.223
Normal-to-shear stiffness ratio	1.2	1.05	1.0	1.0	1.0
Bond normal-to-shear stiffness ratio	1.2	1.2	1.2	1.2	1.2
Tensile strength (MPa)	28.49	28.2	27.3	23.39	21.89
Cohesion strength (MPa)	23.74	23.5	22.8	19.99	18.24

(a)

(b)
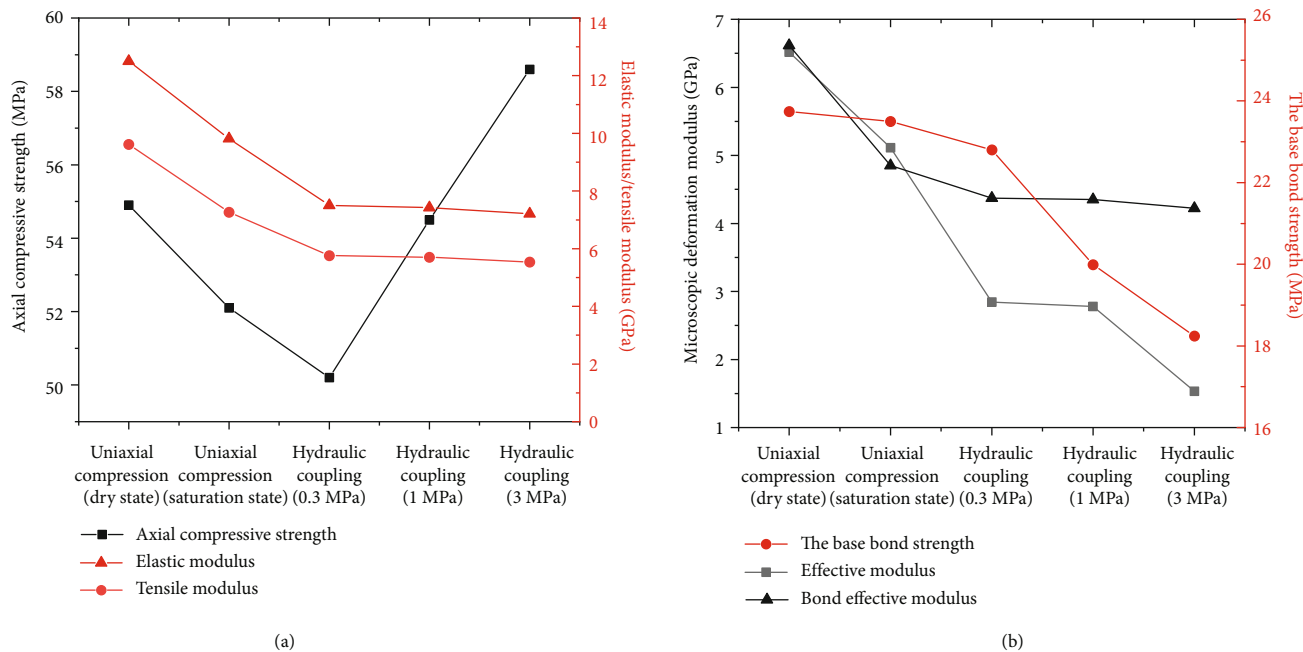
Figure 8: The trends of the parameters related to strength and deformation. (a) Comparison of macroparameters. (b) Comparison of microparameters.
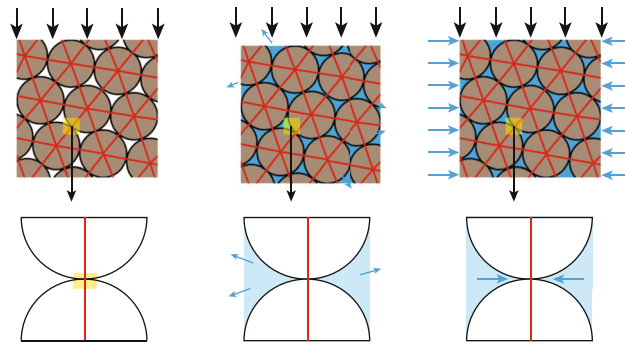
FIGURE 9: The particles under different mechanical states.

(a)   (b)   (c)
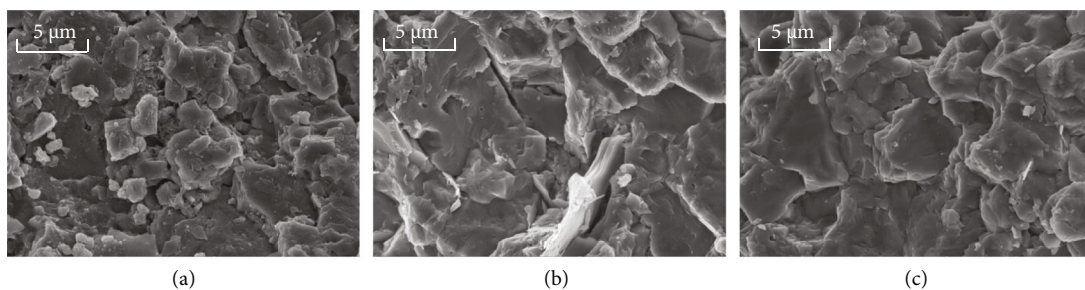
FIGURE 10: Micrographs of the fractured surface under different mechanical states (5000 times magnification). (a) Uniaxial compression in the dry state. (b) Uniaxial compression in the saturated state. (c) Hydraulic coupling under a confining pressure of 1 MPa.

As the rock mass changed from the dry state to the saturated state and then to the hydraulic coupling state, the elastic modulus continued to decrease, while the plastic characteristics continued to strengthen. Microscopically, the effective modulus and the bond effective modulus of the particles decreased. That is, when the degree of water participation increased, the bond effective modulus of the particles decreased under compression and tension. After the bond contact between the particles broke and the parallel bond model degenerated into linear contact, the effective modulus of the particles also decreased. The participation of the water accelerated the deformation between the particles and eventually led to an increase in the plastic deformation of the rock mass.

Similarly, as the degree of water participation increased, the bond contact between the particles became smaller. Furthermore, the number of fractures between the particles increased, which accelerated the destruction of the rock mass and eventually led to a decrease in the peak strength.

3. Discussion

Based on the mechanical state revealed by the laboratory experiments and the numerical simulations, the mechanical mechanism between the rock particles under different mechanical states can be further discussed (Figure 9).

In the saturated state, when the space occupied by the water was compressed, the water was transported, causing the water to have a limited impact on the particle contacts. In the hydraulic coupling state, the compression of storage space did not affect the water pressure. Moreover, the continuous existence of water pressure accelerated the breaking of the contact bond between the particles and further promoted the extension of these microcracks. This was the reason of the difference in the mechanical properties between the saturated state and the hydraulic coupling state.

As the water pressure increased from 0.3 MPa to 1 MPa and then increased to 3 MPa, the micromechanical parameters continued to decrease, even though the macromechanical strength increased. This phenomenon generated because the increase in the water pressure restricted deformation to a certain extent and further weakened the bond contacts between the particles. It should be noted that the reduction in the elastic modulus on the macroparameters was relatively small. When the contact broke into the microcracks, the increase in the water pressure had little effect on the bond effective modulus between the particles, but it had a more significant impact on the effective modulus.

The results of scanning electron microscopy (SEM) of the samples under different mechanical states were selected for comparative analysis (Figure 10). Note that the chosen micrographs were taken from the fractured surface of the rock mass.

The observations of the microstructures revealed that the fracture surface in the dry state was rough, with more loose material. The content of the loose material was the smallest in the hydraulic coupling state, followed by the saturated state. When the degree of water participation was higher, the energy needed to break the bond between the particles was lower; the fractured surface was relatively smooth; and fewer free particles were generated. This phenomenon not

only demonstrated that it is feasible to establish a micro-to-macro link through numerical simulation but it also provided an evidence to the special mechanical state of hydraulic coupling.

As for the high-steep rocky bank, the weak base rock mass in the degradation zone is the key to the overall instability. When considering the changes in the reservoir water level, the evolution of the high-steep rocky bank will become more complicated. It can be found that the change in the hydraulic coupling confining pressure leads to continuous changes in the plastic characteristics of the foot of the rocky bank. And this change in the mechanical state may accelerate the degradation rate of the rock mass.

4. Conclusions

Based on the generalized mechanical model, the newly developed test equipment, numerical simulation, and SEM were used to perform the cross-scale study of the high-steep rocky banks under different mechanical states. And the conclusions can be obtained as follows:

(1) The deformation of high-steep rocky bank was affected by the self-weight of overlying rock mass and induced by the fluctuation of the reservoir water. In this paper, uniaxial compression tests were used to simulate the dry state of the rock mass, and hydraulic coupling tests with different water pressures were used to simulate the rise and fall of the water level. These tests could reflect the increasing axial pressure and the progressive deformation of high-steep rocky bank

(2) As the rock mass changed from the dry state to the saturated state and then to the hydraulic coupling state, its strength continued to decrease, and its plastic characteristics continued to strengthen. The participation of water reduced the bond contact and accelerated the deformation between the particles, eventually leading to an increase in the plastic deformation and a decrease in the peak strength

(3) There were differences in the mechanical properties of the rock mass under the saturated state and the hydraulic coupling state. In the hydraulic coupling state, the water was not transferred due to the compression of storage space, and the water pressure continued to weaken the contact bond between the particles. Therefore, the hydraulic coupling state could accelerate the breaking of the bonds between the particles and further promote the extension of the microcracks

(4) The increase in water pressure restricted the deformation of the rock mass to a certain extent and further weakened the bonds between the particles, which led to an increase in the peak intensity and a reduction of the microparameters. When considering the fluctuations of the reservoir water, this change in the mechanical state may accelerate the degradation rate of the rock mass

Data Availability

The data used to support the findings of this study are available from the corresponding author upon request.

Conflicts of Interest

The authors declare that they have no conflicts of interest.

Acknowledgments

References

[1] H. M. Tang, J. Wasowski, and C. H. Juang, "Geohazards in the three Gorges Reservoir Area, China - Lessons learned from decades of research," *Engineering Geology*, vol. 261, article 105267, 2019.

[2] Y. P. Yin, B. L. Huang, W. P. Wang et al., "Reservoir-induced landslides and risk control in Three Gorges Project on Yangtze River, China," *Journal of Rock Mechanics and Geotechnical Engineering*, vol. 8, no. 5, pp. 577–595, 2016.

[3] L. Q. Wang, J. H. Wu, W. G. Zhang, L. Wang, and W. Cui, "Efficient seismic stability analysis of embankment slopes subjected to water level changes using gradient boosting algorithms," *Frontiers in Earth Science*, vol. 9, article 807317, 2021.

[4] L. Q. Wang, Z. H. Zhang, B. L. Huang, M. J. Hu, and C. Y. Zhang, "Triggering mechanism and possible evolution process of the ancient Qingshi landslide in the Three Gorges Reservoir," *Geomatics, Natural Hazards and Risk*, vol. 12, no. 1, pp. 3160–3174, 2021.

[5] D. M. Gu, H. L. Liu, X. C. Gao, D. Huang, and W. G. Zhang, "Influence of cyclic wetting-drying on the shear strength of limestone with a soft interlayer," *Rock Mechanics and Rock Engineering*, vol. 54, no. 8, pp. 4369–4378, 2021.

[6] B. L. Huang, Y. P. Yin, G. Q. Yan, B. Li, Z. Qin, and J. Wang, "A study on in situ measurements of carbonate rock mass degradation in the water-level fluctuation zone of the Three Gorges Reservoir, China," *Bulletin of Engineering Geology and the Environment*, vol. 80, no. 2, pp. 1091–1101, 2021.

[7] L. Q. Wang, Y. P. Yin, B. L. Huang, Z. H. Zhang, P. Zhao, and Y. J. Wei, "A study of the treatment of a dangerous thick submerged rock mass in the Three Gorges Reservoir Area," *Bulletin of Engineering Geology and the Environment*, vol. 79, no. 5, pp. 2579–2590, 2020.

[8] B. L. Huang, Z. H. Zhang, Y. P. Yin, and F. Ma, "A case study of pillar-shaped rock mass failure in the Three Gorges Reservoir Area, China," *Quarterly Journal of Engineering Geology and Hydrogeology*, vol. 49, no. 3, pp. 195–202, 2016.

[9] L. Q. Wang, B. L. Huang, Z. H. Zhang, Z. W. Dai, P. Zhao, and M. J. Hu, "The analysis of slippage failure of the HuangNanBei slope under dry-wet cycles in the Three Gorges Reservoir

Region, China," *Geomatics, Natural Hazards and Risk*, vol. 11, no. 1, pp. 1233–1249, 2020.

[10] C. Cheng, X. Li, S. D. Li, and B. Zheng, "Failure behavior of granite affected by confinement and water pressure and its influence on the seepage behavior by laboratory experiments," *Materials*, vol. 10, no. 7, p. 798, 2017.

[11] L. B. Meng, T. B. Li, J. Xu, G. Q. Chen, H. M. Ma, and H. Y. Yin, "Deformation and failure mechanism of phyllite under the effects of THM coupling and unloading," *Journal of Mountain Science*, vol. 9, no. 6, pp. 788–797, 2012.

[12] X. G. Wang, Y. P. Yin, J. D. Wang, B. Q. Lian, H. J. Qiu, and T. F. Gu, "A nonstationary parameter model for the sandstone creep tests," *Landslides*, vol. 15, no. 7, pp. 1377–1389, 2018.

[13] Z. K. Wu, J. Zhang, X. Z. Li et al., "Influence of microcracks on stress sensitivity in tight sandstone," *Lithosphere*, vol. 2021, article 7073494, 2021.

[14] L. Q. Wang, Y. P. Yin, C. Y. Zhou, B. L. Huang, and W. P. Wang, "Damage evolution of hydraulically coupled Jianchuandong dangerous rock mass," *Landslides*, vol. 17, no. 5, pp. 1083–1090, 2020.

[15] L. Q. Wang, Y. P. Yin, B. L. Huang, and Z. W. Dai, "Damage evolution and stability analysis of the Jianchuandong dangerous rock mass in the Three Gorges Reservoir Area," *Engineering Geology*, vol. 265, article 105439, 2020.

[16] Z. Liu, C. Y. Zhou, Y. Q. Lu, Z. Z. Lin, and X. F. He, "Development of the multi-scale mechanical experimental system for rheological damage effect of soft rock bearing the hydromechanical coupling action," *Rock and Soil Mechanics*, vol. 39, no. 8, pp. 3077–3086, 2018.

[17] C. Y. Zhou, Y. Q. Lu, Z. Liu, and L. H. Zhang, "An innovative acousto-optic-sensing-based triaxial testing system for rocks," *Rock Mechanics and Rock Engineering*, vol. 52, no. 9, pp. 3305–3321, 2019.

[18] R. Ulusay, *The Isrm suggested methods for rock characterization, testing and monitoring: 2007-2014*, Springer International Publishing, Switzerland, 2014.

[19] Z. L. Zhou, X. Cai, W. Z. Cao, X. B. Li, and C. Xiong, "Influence of water content on mechanical properties of rock in both saturation and drying processes," *Rock Mechanics and Rock Engineering*, vol. 49, no. 8, pp. 3009–3025, 2016.

[20] Y. P. Yin, L. Q. Wang, W. G. Zhang, and Z. W. Dai, "Research on the collapse process of a thick-layer dangerous rock on the reservoir bank," *Bulletin of Engineering Geology and the Environment*, vol. 81, article 109, 2022.

[21] X. R. Liu, Z. J. Wang, Y. Fu, W. Yuan, and L. L. Miao, "Macro/microtesting and damage and degradation of sandstones under dry-wet cycles," *Advances in Materials Science and Engineering*, vol. 2016, Article ID 7013032, 16 pages, 2016.

[22] G. Scaringi, X. M. Fan, Q. Xu et al., "Some considerations on the use of numerical methods to simulate past landslides and possible new failures: the case of the recent Xinmo landslide (Sichuan, China)," *Landslides*, vol. 15, no. 7, pp. 1359–1375, 2018.

[23] Y. Zhuang, A. G. Xing, Y. Leng et al., "Investigation of characteristics of long runout landslides based on the multi-source data collaboration: a case study of the Shuicheng Basalt Landslide in Guizhou, China," *Rock Mechanics and Rock Engineering*, vol. 54, no. 8, pp. 3783–3798, 2021.

[24] F. M. Huang, Z. Ye, J. S. Huang, S. H. Jiang, Z. L. Chang, and J. W. Chen, "Uncertainty study of landslide susceptibility prediction considering the different attribute interval numbers of environmental factors and different data-based models," *Catena*, vol. 202, article 105250, 2021.

[25] T. Xiao, L. B. Yu, W. M. Tian, C. Zhou, and L. Q. Wang, "Reducing local correlations among causal factor classifications as a strategy to improve landslide susceptibility mapping," *Frontiers in Earth Science*, vol. 9, article 781674, 2021.

[26] P. P. Guo, X. N. Gong, Y. X. Wang, H. Lin, and Y. L. Zhao, "Minimum cover depth estimation for underwater shield tunnels," *Tunnelling and Underground Space Technology*, vol. 115, article 104027, 2021.

[27] X. D. Xu, X. B. Cui, X. Liu, Q. Q. Tang, X. H. Zhang, and Y. H. Sun, "Damage analysis of soaking gypsum and safety evaluation of goaf: based on energy dissipation theory," *Geotechnical and Geological Engineering*, vol. 38, no. 6, pp. 6177–6188, 2020.

[28] S. Q. Liu, H. L. Wang, Q. X. Meng, and L. Yan, "Simulating crack development and failure characteristic of toppling rock slope under seismic loading on Lancang River in China," *Lithosphere*, vol. 2021, article 5424127, 2021.

[29] M. H. Mehranpour, P. H. S. W. Kulatilake, X. G. Ma, and M. C. He, "Development of new three-dimensional rock mass strength criteria," *Rock Mechanics and Rock Engineering*, vol. 51, no. 11, pp. 3537–3561, 2018.

[30] P. A. Cundall, "A Computer Model for Simulating Progressive Large Scale Movements in Blocky Rock Systems," in *Proceedings of the Symposium of the International Society for Rock Mechanics, Society for Rock Mechanics (ISRM)*, France, II-8, 1971.

[31] R. Hart, P. A. Cundall, and J. Lemos, "Formulation of a three-dimensional distinct element model–Part II. Mechanical calculations for motion and interaction of a system composed of many polyhedral blocks," *International Journal of Rock Mechanics and Mining Sciences & Geomechanics Abstracts*, vol. 25, no. 3, pp. 117–125, 1988.

[32] D. O. Potyondy, "The bonded-particle model as a tool for rock mechanics research and application: current trends and future directions," *Geosystem Engineering*, vol. 18, no. 1, pp. 1–28, 2015.